



LAWRENCE
LIVERMORE
NATIONAL
LABORATORY

Robust Algorithm for Computing Statistical Stark Broadening of Spectral Lines

Carlos A. Iglesias, Vijay Sonnad

February 12, 2010

High Energy Density Physics

Disclaimer

This document was prepared as an account of work sponsored by an agency of the United States government. Neither the United States government nor Lawrence Livermore National Security, LLC, nor any of their employees makes any warranty, expressed or implied, or assumes any legal liability or responsibility for the accuracy, completeness, or usefulness of any information, apparatus, product, or process disclosed, or represents that its use would not infringe privately owned rights. Reference herein to any specific commercial product, process, or service by trade name, trademark, manufacturer, or otherwise does not necessarily constitute or imply its endorsement, recommendation, or favoring by the United States government or Lawrence Livermore National Security, LLC. The views and opinions of authors expressed herein do not necessarily state or reflect those of the United States government or Lawrence Livermore National Security, LLC, and shall not be used for advertising or product endorsement purposes.

Robust Algorithm for Computing Statistical Stark Broadening of Spectral Lines

CARLOS A. IGLESIAS AND VIJAY SONNAD
Lawrence Livermore National Laboratories
P.O. Box 808, Livermore, CA 94550, USA

Abstract

A method previously developed to solve large-scale linear systems is applied to statistical Stark broadened line shape calculations. The method is formally exact, numerically stable, and allows optimization of the integration over the quasi-static field to assure numerical accuracy. Furthermore, the method does not increase the computational effort and often can decrease it compared to the conventional approach.

PACS:

32.70Jz

Keywords:

Line shape; Stark broadening

Corresponding author:

e-mail: iglesias1@llnl.gov (C. A. Iglesias)

1. Introduction

In standard Stark broadening theory of spectral lines, the perturbing ions are assumed to have negligible motion during the average lifetime of the radiating states [1,2]. In this theory an atom or ion (henceforth the radiator) emits or absorbs radiation in a statistical fluctuating electric field produced by the slow-moving ions. Thus, the line shape involves averaging the Stark state mixing and level splitting over the probability distribution for the quasi-static field [3,4]. In the absence of external fields to define a preferred direction, the line shape can be written in the form [1-4],

$$I(\omega) = \int_0^{\infty} d\varepsilon P(\varepsilon) J(\omega; \varepsilon) \quad (1.1)$$

where $\hbar\omega$ is the energy of the emitted or absorbed photon, $P(\varepsilon)$ is the probability of finding a Stark field of magnitude ε at the radiator, and $J(\omega; \varepsilon)$ represents the line shape due to electron-radiator interactions in the presence of this field.

The numerical evaluation of the line shape replaces the integral in Eq. (1.1) with the sum

$$I(\omega) = \sum_{i=1}^{N_\varepsilon} w_i P(\varepsilon_i) J(\omega; \varepsilon_i) \quad (1.2)$$

where N_ε is the number of field points and w_i are weights that depend on the integration scheme. The calculation of Eq. (1.2) poses a challenge when selecting the field mesh. Firstly, for the integration to yield accurate results the mesh must resolve any narrow features in $J(\omega; \varepsilon)$. Since the structure of $J(\omega; \varepsilon)$ is usually not known *a priori*, a large number of field points are required. Secondly, the conventional method involves an explicit matrix inversion [5-8], which is computationally expensive for large matrices, scaling as m^3 operations for a matrix of size m [9], so there is a premium for defining a mesh with a large number of points.

Often the practical resolution of these contending needs, even for simple one- or two-electron radiators, is a fixed mesh that is sparsely spaced at large field values compromising the accuracy of the integration; particularly in the line wings [10]. Similar compromises are made for line shape calculations of multi-electron systems [10,11] and possible errors from inadequate field meshes may be difficult to identify due to the complexity of the spectrum.

The purpose here is to apply an approach previously developed for large-scale linear systems [12,13] to statistical Stark line broadening. The method is exact in principle, numerically stable, and reveals the resonant structure of $J(\omega; \varepsilon)$ through a dispersion formula allowing optimization

of the numerical integration over the Stark field at each photon frequency. Furthermore, the computational speed for the proposed method is equal to or faster than the conventional approach.

The discussion begins with a brief introduction to Stark line broadening theory in Section 2. Then descriptions of two related methods are given in Sections 3 and 4, respectively, followed by a numerical example in Section 5. Conclusions are offered in the last section.

2. Stark broadening theory

The field-dependent line shape function appearing in standard Stark-broadening theory in Eq. (1.1) can be written in the form [1,2,5-8]

$$\begin{aligned} J(\omega; \varepsilon) &= -\pi^{-1} \text{Im} \text{Tr} \left\{ \vec{d} \cdot R(\omega; \varepsilon) \rho \vec{d} \right\} \\ &= -\pi^{-1} \text{Im} \text{Tr} \left\{ \vec{d} \cdot \vec{x}(\omega; \varepsilon) \right\} \end{aligned} \quad (2.1)$$

where Tr denotes a trace over the radiator internal states with ρ and \vec{d} the radiator density matrix and dipole operators, respectively. The resolvent is defined by its inverse

$$R^{-1}(\omega; \varepsilon) = A(\omega) - \varepsilon B \quad (2.2)$$

where the field independent contribution to the line shape is given by

$$A(\omega) = \Delta\omega - \Phi(\omega), \quad (2.3)$$

$$\Delta\omega y = [\omega - H, y] \quad , \quad (2.4)$$

and the matrix coefficient to the quasi-static field is

$$By = \hbar^{-1} [d_z, y]. \quad (2.5)$$

Here, y is an arbitrary operator in the radiator subspace, $[\dots, \dots]$ denotes a commutator, H is the Hamiltonian for the internal states of the radiator, and the electric field has been chosen along the z-axis. The “width and shift” operator, $\Phi(\omega)$, contains the plasma electron contribution to the relaxation processes of the radiator states [1,2].

The evaluation of the line shape requires radiator energy levels and reduced dipole matrix elements usually obtained from atomic data calculations [14-16]. With these data, together with the description for electron collisional excitations, the matrices above are constructed. The calculation usually proceeds with an explicit matrix inversion to obtain $R(\omega; \varepsilon)$ [1,2]. Thus, for each block of size m the total count of complex number operations at a given frequency is

$$N_i = N_\varepsilon m^3 \quad (2.6)$$

Incidentally, Eq. (2.1) introduced the vector $\vec{x}(\omega; \varepsilon)$ that satisfies the system of equations

$$R^{-1}(\omega; \varepsilon) \vec{x}(\omega; \varepsilon) = \rho \vec{d} \quad (2.7)$$

and is amenable to a variety of techniques. For example, solution of Eq. (2.7) by LU factorization of $R^{-1}(\omega; \varepsilon)$ is 3 times faster than explicit inversion to obtain $R(\omega; \varepsilon)$ [9].

The form of $R^{-1}(\omega; \varepsilon)$ in Eq. (2.2) is suitable for techniques previously developed in large-scale linear systems [12,13] where the quasi-static Stark field is the independent variable. Two approaches are discussed below. The first is based on the eigenvector decomposition and serves to illustrate the advantages of these methods. The second relies on the Hessenberg decomposition, which for large matrices is preferred since it is numerically faster and stable compared to the eigenvector approach.

3. Eigenvector decomposition

The method relies on the eigenvector decomposition of Eq. (2.7), but not of $R^{-1}(\omega; \varepsilon)$ as was done formally in the past [6]. The approach exploits the functional form in Eq. (2.2) to extract the field dependence of $J(\omega; \varepsilon)$ in an efficient manner.

3.1 Method

For each frequency and each $m \times m$ diagonal block, rewrite the trace in the field-dependent line shape expression, (in the following the ω dependence is suppressed for brevity)

$$\begin{aligned} \text{Tr} \left\{ \vec{d} \cdot [A - \varepsilon B]^{-1} \rho \vec{d} \right\} &= \left(\vec{d}^* \right)^T \cdot [I - \varepsilon C]^{-1} A^{-1} \rho \vec{d} \\ &= \left(\vec{d}^* \right)^T P \cdot \vec{v}(\varepsilon) \end{aligned} \quad (3.1.1)$$

where on the right hand side the trace was performed and the notation implies matrix algebra in “line space” [1,2]. Then I is the identity matrix and superscript T denotes transpose in line space, while $*$ denotes Hermitian conjugate in the radiator subspace. The vector $\vec{v}(\varepsilon)$ satisfies

$$[I - \varepsilon \Lambda] \vec{v}(\varepsilon) = P^{-1} A^{-1} \rho \vec{d} \quad (3.1.2)$$

where Λ is a diagonal matrix with entries $\{\lambda_1, \lambda_2, \dots, \lambda_m\}$ that are the eigenvalues of C with

$$C = A^{-1} B = P \Lambda P^{-1} \quad (3.1.3)$$

and the columns of P are the eigenvectors. It is stressed that since C is not Hermitian, the similarity transformation in Eq. (3.1.3) is not unitary; that is, $P^{-1} \neq P^h$, where the superscript h denotes the Hermitian conjugate in line space.

After straightforward manipulation of Eq. (3.1.1), the field-dependent line shape function in Eq. (2.1) can be written as sums over zero and non-zero eigenvalues,

$$J(\omega; \varepsilon) = J_o + \pi^{-1} \sum_{\substack{j \\ (\lambda_j \neq 0)}} \frac{f_j \sigma_j'' + g_j (\varepsilon - \sigma_j')}{(\varepsilon - \sigma_j')^2 + \sigma_j''^2} \quad (3.1.4)$$

where the contribution from vanishing eigenvalues is given by

$$J_o = -\pi^{-1} \text{Im} \sum_{\substack{j \\ (\lambda_j = 0)}} \vec{d}_j^* \cdot [A^{-1} \rho \vec{d}]_j, \quad (3.1.5)$$

the weight of the components in the dispersion formula are

$$\begin{Bmatrix} f_j \\ g_j \end{Bmatrix} = \begin{Bmatrix} \text{Re} \\ \text{Im} \end{Bmatrix} \left\{ \lambda_j^{-1} \left[\left(\vec{d}^* \right)^T P \right]_j \cdot \left[P^{-1} A^{-1} \rho \vec{d} \right]_j \right\}, \quad (3.1.6)$$

and

$$\lambda_j^{-1} = \sigma_j = \sigma_j' + i \sigma_j'' \quad (3.1.7)$$

defines the real and imaginary parts of the poles in the ε complex plane.

3.2 The $A(\omega)$ matrix

The eigenvalue decomposition requires that $A^{-1}(\omega)$ exist. This is always the case since $A(\omega)$ represents the line shape in the absence of a quasi-static Stark field and has non-zero eigenvalues. Furthermore, the interference terms are often neglected making $A(\omega)$ diagonal [5-8]. In any case, all explicit inversions are avoided by solving the linear equations

$$AC = B \quad (3.2.1)$$

$$A\vec{u} = \rho \vec{d} \quad (3.2.2)$$

$$P\vec{z} = \vec{u} \quad (3.2.3)$$

by LU factorization or other techniques. For example, Eqs. (3.3.1) and (3.3.2) may be efficiently solved with sparse matrix iterative schemes [17].

3.3 Efficient Stark field mesh

An advantage of the method is the dispersion formula in Eq. (3.1.4) that defines the structure of $J(\omega; \varepsilon)$; σ_k' locates the center and σ_k'' the half width at half maximum of the k^{th} resonance in $J(\omega; \varepsilon)$. Thus, the number of points in the Stark field integration can be optimized. For example,

the minimal set of points necessary to resolve the distribution function $P(\varepsilon)$ is, if necessary, supplemented with points to resolve $J(\omega; \varepsilon)$ obtained from knowledge of the poles.

3.4 Operation count

The operation count determines the relative costs of an algorithm. Although the matrices A and B are typically sparse, it is expedient to ignore this property to obtain conservative estimates of the relative computational efficiencies. In the following, all counts assume operations performed with complex numbers.

The eigenvalue decomposition requires $27m^3$ operations, which is considerably more operations than a single matrix inversion [9]. On the other hand, only m operations are necessary to solve Eq. (3.1.2) at each field value. In addition, the solution of Eqs. (3.2.1) through (3.2.3) requires two LU factorizations with $m+2$ right hand sides leading to $\sim 2m^3$ operations. Thus, the total operations of the eigenvector decomposition at each frequency is

$$N_v = 29m^3 + N_\varepsilon m \quad (3.4.1)$$

to be compared with Eq. (2.6).

4. Hessenberg method

The eigenvector decomposition is an expensive procedure that may also suffer from numerical instability for ill-conditioned matrices [9]. It is possible to take advantage of the ideas in Sect. 3 using the numerically stable Hessenberg decomposition together with the QR algorithm [9,12,13].

4.1 Hessenberg decomposition

The Hessenberg decomposition is defined as [9]

$$C = QWQ^h \quad (4.1.1)$$

where Q is a unitary matrix and W is an upper Hessenberg matrix (i.e.; $W_{ij} = 0$ for $i > j+1$).

Following manipulations similar to those leading to Eq. (3.1.1) yields

$$\left(\vec{d}^*\right)^T \cdot [A - \varepsilon B]^{-1} \rho \vec{d} = \left(\vec{d}^*\right)^T Q \cdot \vec{s}(\varepsilon) \quad (4.1.2)$$

$$[1 - \varepsilon W] \vec{s}(\varepsilon) = Q^h \rho \vec{d}, \quad (4.1.3)$$

and the procedure again avoids explicit inversion by using Eqs. (3.2.1) and (3.2.2).

4.2 Operation count

The Hessenberg decomposition together with the QR algorithm to obtain eigenvalues and unitary transformation involves $10m^3$ operations for a matrix of size m [9]. On the other hand,

the solution of Eq. (4.1.3) using LU factorization takes m^2 operations rather than m as in the eigenvector approach [13]. Thus, the total operation count at each frequency, including solving Eqs (3.2.1) through (3.2.2), is

$$N_w = 12m^3 + N_\epsilon m^2 \quad (4.2.1)$$

which is less than N_v in Eq. (3.4.1) for large m .

Comparing the operational count of the Hessenberg method to explicit inversion yields from Eqs. (2.6) and (4.2.1)

$$\frac{N_w}{N_i} = \frac{12 + \frac{N_\epsilon}{m}}{N_\epsilon} \xrightarrow{N_\epsilon \ll m} \frac{12}{N_\epsilon} < 1 \quad (4.2.2)$$

since typically $N_\epsilon \geq 30$ [10,11]. Note that the ratio in Eq. (4.2.2) would be increased by a factor of 3 when comparing to a solution of Eq. (2.7) by LU factorization. In that case the Hessenberg decomposition approach is approximately comparable in speed, however, there is the benefit in the Hessenberg method of advance knowledge concerning the field-dependent resonances.

4.3 Numerical issues

Although the matrix $A(\omega)$ is non-singular, it may be ill-conditioned and solving the linear systems in Eqs. (3.2.1) and (3.2.2) could lead to inaccurate results. As an alternative, the generalized Schur decomposition can be applied to matrices $A(\omega)$ and B . Even though B can be a singular matrix, this is a numerically stable algorithm requiring $\sim 66m^3$ operations [9]. Nevertheless, it may be the best alternative for numerically difficult cases. Note that the generalized Schur decomposition provides the eigenvalues and requires m^2 operations to solve the simultaneous equations at each field value. Incidentally, the Schur decomposition can be applied to the matrix $C(\omega)$ leading to similar results as those in Sect. 4.1. Although it is also numerically stable, the Schur decomposition requires about twice the number of operations as the Hessenberg method [9,12,13].

5. Numerical example

As an example, it is well known that the far line wing of one-electron radiators involves large Stark field values. In line shape calculations compromises are often made in order to minimize the numerical effort by using a widely spaced field mesh in the tail of the distribution [9,10]. Specifically, results for the Stark shifted components of the hydrogen Lyman- α line are plotted in

Fig. 1 where the details of the calculation are provided in the Appendix. Briefly, in one case the integration over the microfield distribution uses a fixed field mesh while the second calculation has a flexible mesh that resolves the resonance in $J(\omega; \epsilon)$ at each frequency. Figure 1 clearly shows that the flexible mesh produces a smooth line wing while the fixed mesh yields large oscillations beyond a certain detuning frequency.

The results in Fig. 1 are readily explained by considering the resonant structure of $J(\omega; \epsilon)$. A plot of $J(\omega; \epsilon)$ at $\Delta\omega = 0.001 \text{ eV}$ in Fig. 2 shows that the fixed mesh resolves the resonant feature at this frequency. Therefore, the resulting profile near line center is numerically accurate. At much larger detuning frequencies, however, the fixed mesh fails to resolve the resonance as shown in Figs. 3 and 4. As a result, the fixed mesh integration can overestimate or underestimate the correct value leading to the oscillatory behavior in Fig. 1.

The example is intentionally simple and clearly illustrates the advantages of determining the resonant structure of the field-dependent line shape. In more complex problems involving multi-electron radiators the fixed field mesh may be inadequate [5]; however, due to the complexity of the spectrum, errors may be difficult to detect. By using the Hessenberg method in Sect. 4 it is possible to judiciously add field points and achieve accurate integration without unduly increasing the computational effort. Note that the added points may include extension of the integration range, which otherwise may be completely missed using a fixed field mesh.

6. Conclusion

A robust numerical algorithm for calculating statistical Stark broadened spectral lines without introducing approximations or increasing the computational effort was proposed. The method evaluates the field-dependent line shape using the Hessenberg decomposition of a field independent matrix and the solution to a system of simultaneous linear equations. As a result, the number of operations to compute the field-dependent line shape for a diagonal block of size m at each field value is m^2 compared to m^3 in the conventional approach.

An important advantage of the proposed method is identification of the resonant structure in the field-dependent line shape. Thus, it is possible to optimize the field mesh at each frequency when performing the integration over the microfield distribution leading to improved numerical accuracy while minimizing the computational effort.

Acknowledgments: It is pleasure to thank Richard W. Lee for valuable discussions. This work performed under the auspices of the U.S. Department of Energy by Lawrence Livermore National Laboratory under Contract DE-AC52-07NA27344.

Appendix

Calculation of Lyman- α line

The Lyman- α spectral line describes a radiative transition between principal quantum numbers $n=2$ and $n=1$ in the hydrogen atom. In the present calculations all interactions between states with different principal quantum numbers are neglected simplifying the matrix algebra. The resulting matrix involving the upper 4 states reduces to block diagonal form: a 2x2 block plus 2 (1x1) blocks. Therefore, analytical expression can be readily obtained.

A.1 Line shape function

The line shape function can be written in the form,

$$I(\omega) = S \left\{ 2I^{(1)}(\omega) + I^{(o)}(\omega) \right\} \quad (\text{A.1.1})$$

where S is the total line strength. The first term is the area normalized profile for the unshifted 2p states with magnetic quantum number $|m|=1$ that are not affected by the quasi-static Stark field,

$$I^{(1)}(\omega) = \frac{\gamma(\omega)/\pi}{\Delta\omega + \gamma^2(\omega)} \quad (\text{A.1.2})$$

The second term is the contribution from the 2s and 2p states with $m=0$ that couple through the Stark field,

$$I^{(o)}(\omega) = \int_o^\infty d\varepsilon P(\varepsilon) J^{(o)}(\omega; \varepsilon) \quad (\text{A.1.3})$$

with

$$J^{(o)}(\omega; \varepsilon) = -\pi^{-1} \text{Im} \left\{ \frac{\Delta\omega + 3i\gamma(\omega)}{[\Delta\omega + i\gamma(\omega)][\Delta\omega + 3i\gamma(\omega)] + [3ea_o\varepsilon/\hbar]^2} \right\} \quad (\text{A.1.4})$$

where a_o is the Bohr radius and e the elemental electric charge.

A.2 Poles of $J^{(o)}(\omega; \varepsilon)$

The eigenvector decomposition can be applied to the Lyman- α example. For the $m=0$ block, Eqs. (2.3)-(2.5) yield

$$A(\omega) = \begin{bmatrix} \Delta\omega + 3i\gamma & 0 \\ 0 & \Delta\omega + i\gamma \end{bmatrix} \quad (\text{A.2.1})$$

and

$$B = \frac{3ea_o}{\hbar} \begin{bmatrix} 0 & 1 \\ 1 & 0 \end{bmatrix} \quad (\text{A.2.2})$$

leading to

$$C = A^{-1}B = \frac{3ea_o\hbar^{-1}}{\Delta\omega^2 - 3\gamma^2 + 4i\Delta\omega\gamma} \begin{bmatrix} 0 & (\Delta\omega + i\gamma) \\ (\Delta\omega + 3i\gamma) & 0 \end{bmatrix} \quad (\text{A.2.3})$$

The eigenvalues of C are given by

$$\lambda(\omega) = \pm \frac{3ea_o}{\hbar\sqrt{(\Delta\omega + i\gamma)(\Delta\omega + 3i\gamma)}} \quad (\text{A.2.4})$$

Thus, from Eq. (3.1.7) the poles of $J^{(o)}(\omega;\varepsilon)$ are

$$\sigma(\omega) = \pm \frac{\hbar}{3ea_o} \left\{ \left(\Delta\omega^2 - 3\gamma^2 \right)^2 + 16\Delta\omega^2\gamma^2 \right\}^{1/4} \left\{ \cos\left(\frac{\theta(\omega)}{2}\right) + i \sin\left(\frac{\theta(\omega)}{2}\right) \right\} \quad (\text{A.2.5})$$

with

$$\theta(\omega) = \text{Arg}[\Delta\omega^2 - 3\gamma^2 + 4i\Delta\omega\gamma] \quad (\text{A.2.6})$$

As an example, consider $\Delta\omega = 0$. Then $\theta(\Delta\omega = 0) = -\pi$ leading to $\sigma(\Delta\omega = 0) = \pm i\hbar\gamma/\sqrt{3}ea_o$.

A.3 Calculations

The present calculations used a standard approximation for the width, $\gamma(\omega)$, [18] and the necessary reduced dipole matrix elements are readily available [19]. For simplicity, the integration used the Holtsmark microfield distribution [3] with a trapezoidal rule. The fixed mesh integration used $N_\varepsilon = 60$ field points in a predetermined grid [20]. No systematic effort was made to optimize the mesh. Instead, the flexible mesh complemented the fixed grid with 7 uniformly spaced points centered at the peak of the resonance with spacing set equal to the width $\gamma(\omega)$. Both the location and width are obtained from Eqs. (A.2.5) and (A.2.6). This flexible mesh reduced the oscillations in the line wing to less than $\pm 10\%$ compared to $\pm 100\%$ with the fixed mesh.

References

- [1] H.R. Griem, *Spectral Line Broadening by Plasma* (Academic, new York, 1974)
- [2] M. Baranger, *Atomic and Molecular Processes*, ed. D. Bates (Academic Press, New York, 1962)
- [3] J. Holtsmark, *Ann.Phys.* (Leipzig) **7**, 578(1919)
- [4] H. Margeneau & M. Lewis, *Rev.Mod.Phys.* **31**, 569(1959)
- [5] L.A. Woltz & C.F. Hooper, *Phys.Rev.* **38**, 4766(1988)
- [6] R.C. Mancini *et al*, *CPC* **63**, 314(1991)
- [7] A. Calisti *et al*, *Phys.Rev.* **A42**, 5433(1990)
- [8] P.A. Loboda *et al*, *Laser & Particle Phys.* **18**, 275(2000)
- [9] G.H. Golub & C.F. Loan, *Matrix Computations*, (John Hopkins Press, 1996)
- [10] R.W. Lee, (*private communication*)
- [11] R. Mancini, (*private communication*)
- [12] A. Laub, *IEEE Trans. Automatic Control* **26**, 407(1981)
- [13] C.F. Loan, *Math. Programming Study* **18**, 102(1982)
- [14] R. D. Cowan, *The Theory of Atomic Structure and Spectra* (University of California Press, Berkeley, 1981)
- [15] A. Bar-Shalom & M. Klapisch, *Comput.Phys. Commun* **50**, 375(1988)
- [16] F.A. Parpia *et al*, *Comput.Phys. Commun* **94**, 249(1996)
- [17] R.W. Freund & N. Nachtigal, *ACM Trans. Math. Software* **22**, 46(1996)
- [18] H.R. Griem, M. Blaha & P.C. Kepple, *Phys.Rev.* **A19**, 2421(1979)
- [19] B.W. Shore & D.H. Menzel, *ApJS* **12**, 187(1965)
- [20] I.I. Sobelman, L.A. Vainshtein & E.A. Yukov, *Excitation of Atoms and Broadening of Spectral Lines* (Springer-Verlag, Berlin, 1981), pg. 278.

Figure Captions

Fig. 1 Stark shifted components contribution to the hydrogen Lyman- α profile at $T = 1\text{eV}$ and

$N_e = 10^{16}\text{cm}^{-3}$ versus detuning frequency. Calculation using a fixed mesh (*solid*) and with a flexible field mesh to resolve the resonances (*dash*).

Fig. 2 $J^{(o)}(\Delta\omega; \varepsilon)$ for the shifted Stark components of the hydrogen Lyman- α line at conditions of

Fig. 1 versus Stark field in units of the Holtsmark field ε_H [3] at $\Delta\omega = 0.001\text{eV}$. The solid dots represent calculations on a fixed field mesh.

Fig. 3 Same as Fig. 2 at $\Delta\omega = 0.00475\text{eV}$. The dashed line indicates the error using the trapezoidal rule with the fixed mesh.

Fig. 4 Same as Fig. 3 at $\Delta\omega = 0.00525\text{eV}$.

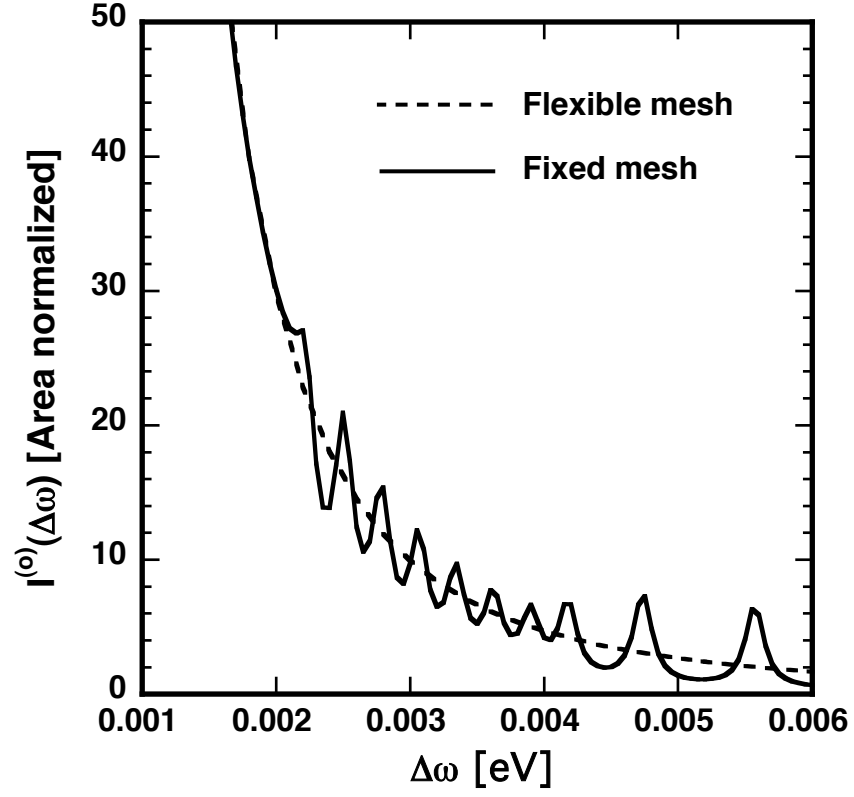


Fig. 1 Stark shifted components contribution to the hydrogen Lyman- α profile at $T=1eV$ and $N_e = 10^{16} cm^{-3}$ versus detuning frequency. Calculation using a fixed mesh (*solid*) and with a flexible field mesh to resolve the resonances (*dash*).

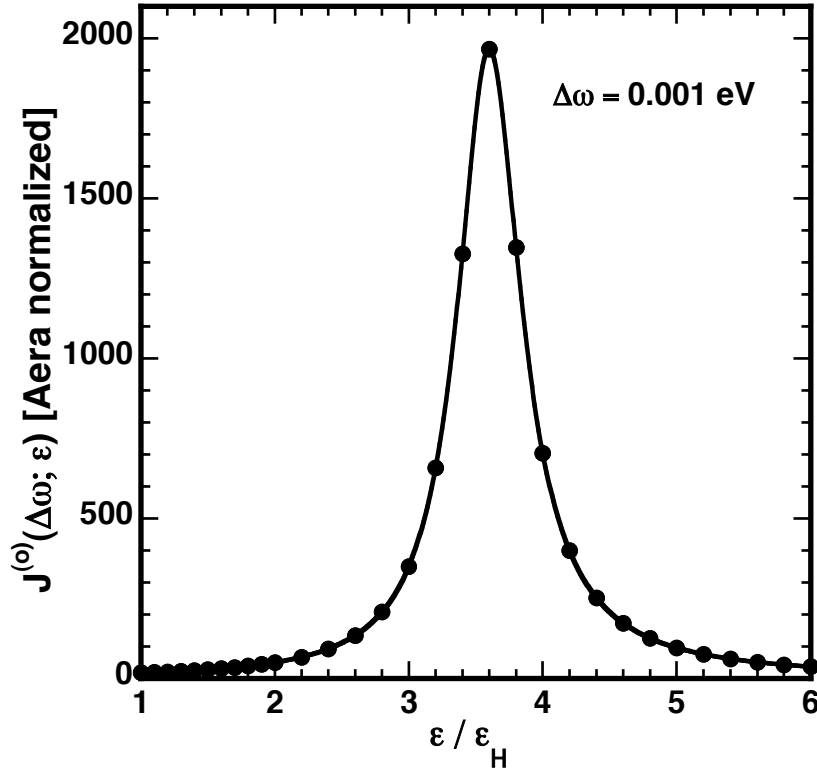


Fig. 2 $J^{(o)}(\Delta\omega; \epsilon)$ for the shifted Stark components of the hydrogen Lyman- α line at conditions of Fig. 1 versus Stark field in units of the Holtsmark field ϵ_H [3] at $\Delta\omega = 0.001 \text{ eV}$. The solid dots represent calculations on a fixed field mesh.

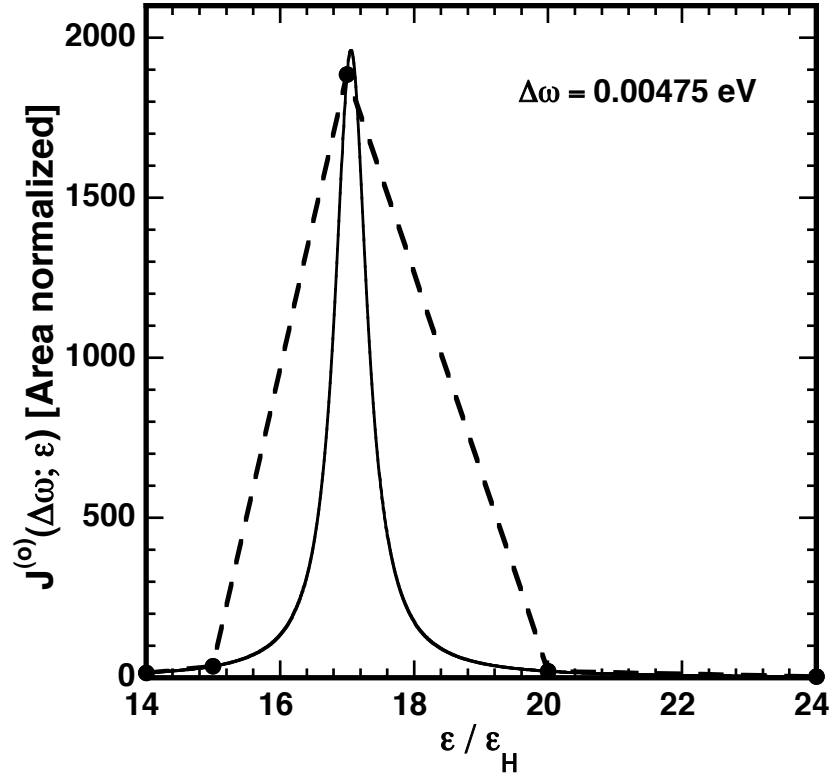


Fig. 3 Same as Fig. 2 at $\Delta\omega = 0.00475$ eV. The dashed line indicates the error using the trapezoidal rule with the fixed mesh.

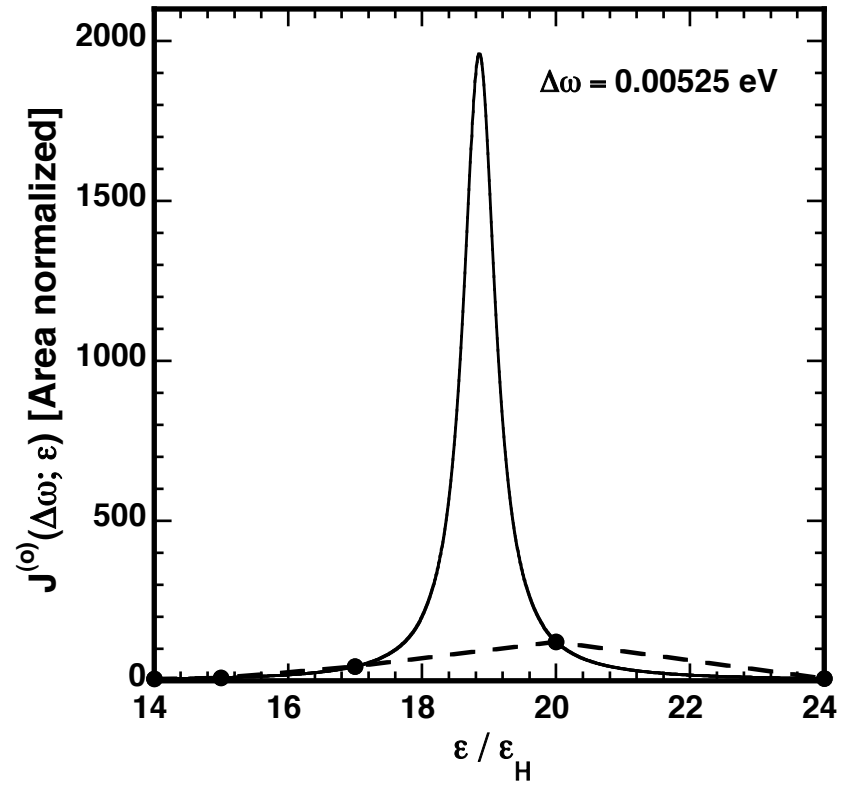


Fig. 4 Same as Fig. 3 at $\Delta\omega = 0.00525 \text{ eV}$.